E-MoFlow: Learning Egomotion and Optical Flow from Event Data via Implicit Regularization

Wenpu Li[1*], **Bangyan Liao**[1,2*], **Yi Zhou**[3], **Qi Xu**[1,4], **Pian Wan**[5], **Peidong Liu**[1†],

[1]Westlake University [2]Zhejiang University
[3]Hunan University [4]Wuhan University [5]Georgia Institute of Technology

Project Page: https://akawincent.github.io/EMoFlow/

Abstract

The estimation of optical flow and 6-DoF ego-motion, two fundamental tasks in 3D vision, has typically been addressed independently. For neuromorphic vision (e.g., event cameras), however, the lack of robust data association makes solving the two problems separately an ill-posed challenge, especially in the absence of supervision via ground truth. Existing works mitigate this ill-posedness by either enforcing the smoothness of the flow field via an explicit variational regularizer or leveraging explicit structure-and-motion priors in the parametrization to improve event alignment. The former notably introduces bias in results and computational overhead, while the latter, which parametrizes the optical flow in terms of the scene depth and the camera motion, often converges to suboptimal local minima. To address these issues, we propose an unsupervised framework that jointly optimizes egomotion and optical flow via implicit spatial-temporal and geometric regularization. First, by modeling camera's egomotion as a continuous spline and optical flow as an implicit neural representation, our method inherently embeds spatial-temporal coherence through inductive biases. Second, we incorporate structure-and-motion priors through differential geometric constraints, bypassing explicit depth estimation while maintaining rigorous geometric consistency. As a result, our framework (called **E-MoFlow**) unifies egomotion and optical flow estimation via implicit regularization under a fully unsupervised paradigm. Experiments demonstrate its versatility to general 6-DoF motion scenarios, achieving state-of-the-art performance among unsupervised methods and competitive even with supervised approaches.

1 Introduction

Optical flow estimation [1] and 6-DoF camera motion recovery [2] are two core building blocks in many 3D vision tasks, playing a crucial role in providing motion and structural information for various downstream applications such as object tracking [3, 4], scene reconstruction [5, 6], and Simultaneous Localization and Mapping (SLAM) [7–9]. In classical computer vision, these two problems have been extensively studied and can be successfully solved independently, thanks to well-established feature extraction techniques [10] and data association [11] algorithms. However, when applied to the emerging field of neuromorphic vision [12], these traditional methods face significant challenges. The unique nature of event cameras [12], which reports asynchronous and sparse events instead of capturing frames, brings challenges in estimating optical flow and 6-DoF camera motion reliably. For example, optical flow estimation from event data faces the well-known aperture problem [13], where the learned flow is essentially the normal flow [14]. Furthermore, depth-free 6-DoF motion

*Equal Contribution: {liwenpu,liaobangyan}@westlake.edu.cn
† Corresponding author: liupeidong@westlake.edu.cn

39th Conference on Neural Information Processing Systems (NeurIPS 2025).

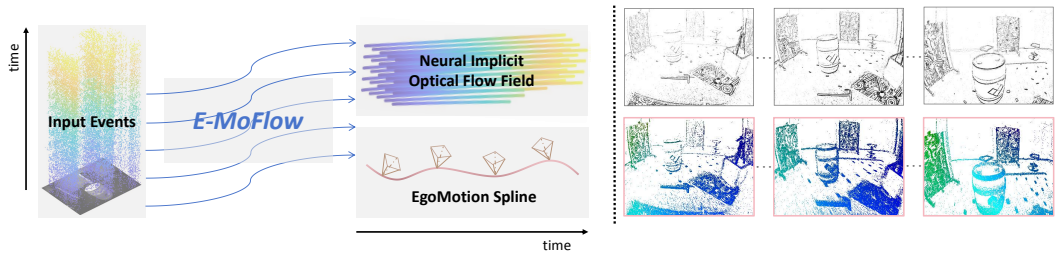

(a) Our method takes input of events, and predicts the dense and continuous optical flow and ego-motion.

(b) Recovered dense optical flow fields and corresponding images of warped events (IWE).

Figure 1: **Illustration of E-MoFlow**.

estimation in general scenes has been proved to be theoretically intractable [15] unless a locally constant depth assumption is imposed on the event data [16]. These challenges stem primarily from the absence of reliable long-term association in event data, rendering independent estimation of these two problems ill-posed and error-prone.

To overcome these challenges, existing approaches have primarily focused on regularization techniques to constrain the inherently ill-posed nature of these problems. One common strategy leverages spatial-temporal regularization to explicitly enforce optical flow continuity over both time and space [17–19]. These methods typically incorporate additional loss terms during optimization, which helps stabilize solutions but introduces trade-offs: the regularization constraints may bias flow estimation while simultaneously increasing computational complexity. In contrast, our approach embeds these regularization priors implicitly through learned representations. We formulate camera egomotion as a spline in the space of first-order kinematics [20] and optical flow as an implicit neural representation [21], which intrinsically encode spatial-temporal continuity. This representation-driven regularization eliminates the need for explicit constraint terms while maintaining solution stability.

Another line of works [16, 19] introduce geometric regularization by jointly estimating motion and depth. These approaches have shown improvements in optical flow accuracy, as depth information provides valuable constraints for motion estimation. However, these methods typically rely on motion fields [22] or re-projection equations [6] to relate optical flow, depth, and camera motion. This explicit depth estimation increases the degrees of freedom in the model, leading to a higher risk of local minima and instability during the optimization process. To address this issue, we adopt differential geometric constraints [23] to jointly estimate egomotion and optical flow without requiring explicit depth estimation. This approach implicitly incorporates geometric regularization, stabilizing the solution while retaining the ability to accurately estimate egomotion and flow.

In summary, **E-MoFlow** as shown in Fig. 1, unifies egomotion and optical flow estimation through implicit regularization under a fully unsupervised learning paradigm. We conduct extensive experiments across a variety of 6-DoF motion scenarios, demonstrating the applicability and robustness of our method. Experimental results demonstrate that **E-MoFlow** outperforms existing unsupervised methods and achieves comparable performance to supervised approaches.

2 Related Work

Event-based Optical Flow Learning Event cameras asynchronously measure per-pixel intensity changes, not absolute values at fixed intervals [12]. This enables high dynamic range and low-latency sensing. However, estimating optical flow from local event patches inherently suffers from the aperture problem [13, 14]. Because traditional optimization-based methods struggle to recover full motion fields from this ambiguous local data, learning-based approaches have become dominant. These learning-based optical flow methods are broadly categorized as supervised, semi-supervised, and unsupervised.

Supervised methods [24–32] rely on dense ground-truth optical flow for training, typically requiring large-scale synthetic or real-world datasets. However, acquiring accurate flow annotations at scale is prohibitively expensive, often leading to a significant sim-to-real gap that restricts their practical deployment in real-world environments. Semi-supervised methods, such as [18, 33, 34], mitigate this limitation by incorporating grayscale images and enforcing photometric consistency as a su-

pervisory signal. While these approaches reduce dependency on labeled data, their performance is highly sensitive to the quality of reconstructed intensity images, making them unreliable in extreme conditions (e.g., high-speed motion or low-light scenarios). In contrast, unsupervised learning methods [17, 19, 27, 32, 35–37] operate solely on event data, eliminating the need for external supervision. These methods typically optimize optical flow using contrast maximization (CMax) objectives [15], which align event warping with estimated motion. Depending on their learning paradigm, unsupervised approaches can be further divided into online and offline fashion. The former (e.g., [27, 32, 35–37]) employs neural networks to predict optical flow directly from event representations (e.g., event images or voxel grids). These approaches enable efficient, real-time inference but may suffer from error accumulation due to their feedforward nature. The latter (e.g., [17]) iteratively refines flow estimates from scratch for each new event batch. While more computationally intensive, this kind of method avoids the limitations of learned feature extraction, though often at the cost of reduced efficiency compared to online techniques.

In this work, we adopt an unsupervised learning paradigm that combines the efficiency of neural networks with high estimation accuracy. Our approach eliminates reliance on labeled data or auxiliary intensity images, ensuring robust performance across diverse and challenging scenarios.

Event Camera Egomotion Estimation Direct egomotion estimation from event streams represents a fundamental yet highly challenging problem in event-based computer vision. Existing approaches primarily follow either 1) linear solver or 2) nonlinear optimization paradigms, each with distinct advantages and limitations.

Linear solver methods employ well-designed geometric constraints to derive closed-form motion solutions. For instance, EvLinearSolver [14] achieves 3-DoF rotation estimation and 6-DoF motion (by incorporating depth priors) through event-based normal flow constraints. Related work by [38, 39] utilizes event-based line features for translation estimation when angular velocity is known. As a result, these methods fundamentally require some form of prior knowledge, preventing complete egomotion recovery from event data alone. On the nonlinear optimization front, contrast-based approaches [15, 40–42] warp events to a reference timestamp and optimize motion parameters by maximizing the contrast in the resulting Image of Warped Events (IWE). While effective for certain motion patterns, these methods face critical challenges including degenerate solutions like event collapse [41] and inherent limitations in recovering full 6-DoF motion without depth priors (or necessarily assuming a constant depth shared by local events). Alternative spatial-temporal registration methods [43–46] leverage time surfaces for motion estimation, offering computational efficiency through sparse event processing but demonstrating increased sensitivity to noise compared to contrast-based techniques. More recently, [47] *et al.* propose an iterative optimization pipeline for 6-DoF motion estimation using event-based line features.

In conclusion, current solutions - whether linear or nonlinear - still cannot achieve reliable 6-DoF motion estimation in general scenarios without restrictive assumptions. This fundamental limitation highlights the need for more robust approaches capable of handling the full complexity of egomotion estimation from event data.

Flow and Motion Joint Estimation Joint estimation of optical flow and camera motion typically builds upon the motion field theory [22] or re-projection constraints [6], which inherently require depth estimation. [19] pioneers an event-based framework using discretized spatial-temporal volumes to jointly predict optical flow and ego-motion, employing motion compensation through motion blur based and temporal re-projection losses for unsupervised learning. Similarly, [48] utilizes the Evenly-Cascaded Convolutional Network to parameterize depth and pose, employing the re-projection error between warped event images and the current frame as a supervisory signal to jointly optimize depth, motion, and optical flow.

A distinct approach is presented by [16], which introduces a contrast maximization framework for simultaneous estimation of optical flow, depth, and egomotion through motion field parameterization. However, these joint estimation methods face a critical challenge: the inclusion of depth estimation expands the parameterization space, introducing additional degrees of freedom that require stronger regularization to avoid convergence to local minima.

Neural Flow Fields Recent studies [21, 49] have demonstrated the significant potential of using deep neural network as continuous and memory-efficient implicit representations for tasks such as view synthesis [50] [51], scene flow estimation [52, 53], and Non-Rigid Structure from Motion [54].

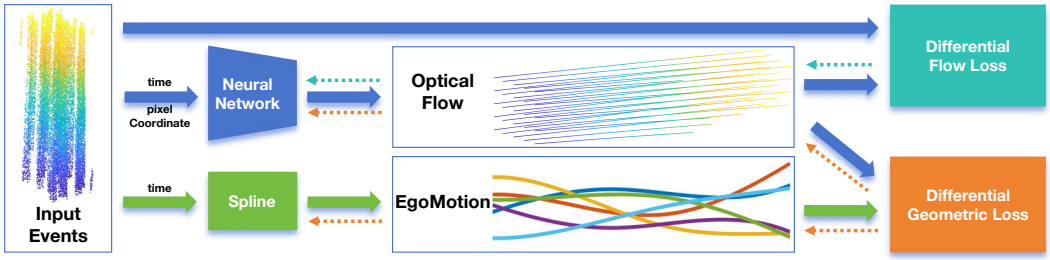

Figure 2: **Training Pipeline of E-MoFlow.** Given the input event data, we use differential flow loss Eq. (8) and differential geometric loss Eq. (9) to train the neural network Eq. (2) and spline parameters Eq. (6). These two losses are optimized together until convergence. Solid arrows denote the forward process; dashed arrows denote gradient backpropagation.

This class of methods leverages coordinate-based networks to store the mapping from spatio-temporal coordinates to target vectors, such as radiance values or motion fields. The inherent smoothness bias of the neural network architecture itself serves as a powerful "neural prior," providing implicit regularization for downstream problems and replacing traditional handcrafted regularizers.

By modeling the differential properties of the scene [52–54], this paradigm can be extended to represent entire temporal dynamics as Ordinary Differential Equations (ODEs) and to estimate complex, long-term 3D trajectories. This provides a solid foundation for our proposed method.

3 Methodology

In this section, we will first introduce the continuous representations of optical flow and camera motion (Sec. 3.1). Next, we will introduce the differential losses used in our work (Sec. 3.2), including differential flow loss Eq. (8) and differential geometric loss Eq. (9). Finally, we summarize our training pipeline in Sec. 3.3.

3.1 Continuous Representations

To include the spatial-temporal consistency prior through continuous representations implicitly, we model ego-motion and optical flow as spline [20] and implicit neural representations [21], respectively.

Continuous Flow. Implicit neural representations [21] model the continuous signal through a spatial-temporal coordinate based neural network. Specifically, given a time t and a normalized pixel coordinate $\mathbf{x}$, the neural network will output a normalized optical flow vector $\mathbf{u}_\theta(t, \mathbf{x})$. We can write it as

$$\mathbf{u}_\theta(t, \mathbf{x}) = \mathrm{NN}_\theta(t, \mathbf{x}), \tag{1}$$

where we denote the parameters of this neural network as θ. The detailed implementation can be found in Sec. 4.1. Besides, following the Neural Ordinary Differential Equation (Neural ODE) [55], we can reformulate the warping trajectory of an event $e_k \doteq \{\mathbf{x}_k, t_k\}$ as a neural ODE solution. In particular, given the initial condition, the warping terminal point at time t can be denoted as $e_k(t) \doteq \{\mathbf{x}_k(t), t\}$ and it satisfies the following equation:

$$\frac{d\mathbf{x}_k(t)}{dt} = \mathrm{NN}_\theta(t, \mathbf{x}_k(t)), \quad \mathbf{x}_k(t_k) = \mathbf{x}_k. \tag{2}$$

This ODE can be integrated by any off-the-shelf ODE solvers (e.g., euler [56], rk4 [57], dopri5 [58]), with the solution defining the event warping trajectory:

$$\mathbf{x}_k(t) = \mathbf{x}_k + \int_{t_k}^{t} \mathrm{NN}_\theta(s, \mathbf{x}_k(s))\, ds \tag{3}$$

For the backward gradient, this can be solved by a reverse adjoint ODE. Given a scalar-valued loss function at the reference time point $L(\mathbf{x}_k(t_{\text{ref}}))$, the adjoint state $\mathbf{a}_k(t) = \mathrm{d}L/\mathrm{d}\mathbf{x}_k(t)$ namely the gradient at time t can be represented by

$$\frac{d\mathbf{a}_k(t)}{dt} = -\mathbf{a}_k(t)^\top \frac{\partial \mathrm{NN}_\theta(t, \mathbf{x}_k(t))}{\partial \mathbf{x}_k(t)}, \quad \mathbf{a}_k(t_{\text{ref}}) = \frac{\mathrm{d}L(\mathbf{x}_k(t_{\text{ref}}))}{\mathrm{d}\mathbf{x}_k(t_{\text{ref}})}. \tag{4}$$

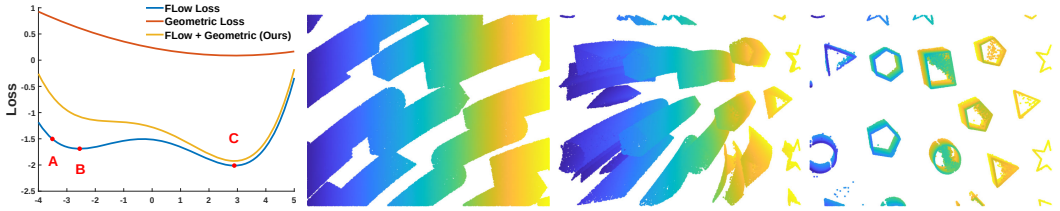

(a) Parameter Landscape (b) Original IWE at A (c) IWE at minimal B (d) IWE at minimal C

Figure 3: **Landscape of different loss functions.** By jointly estimating these two losses, we can avoid getting stuck in local minima, making it possible to solve the ill-posed problem.

Finally, to get the gradient to the parameters, we can perform a simple integral along time as:

$$\frac{dL}{d\theta} = -\int_{t_{\text{ref}}}^{t_k} \mathbf{a}_k(t)^\top \frac{\partial \text{NN}_\theta(t, \mathbf{x}_k(t))}{\partial \theta} dt \tag{5}$$

Remark. Unlike previous work, which directly models displacement [17, 19], our approach directly models optical flow (velocity field). This enables our method to be applicable to scenes with more aggressive motion. Additionally, direct backpropagation of gradients can lead to gradient explosion and excessive memory usage [55]. The Neural ODE [55] approach mitigates this by modeling the backpropagation of gradients as an adjoint ODE, significantly reducing memory consumption.

Continuous Motion. Unlike optical flow, camera ego-motion is low-dimensional, and we represent it using a cubic B-spline [20]. Specifically, given $n+1$ control points $\beta_i \in \mathbb{R}^6$, the angular and linear velocities $\boldsymbol{\omega}_\beta(t), \boldsymbol{\nu}_\beta(t)$ at time t can be derived as follows:

$$[\boldsymbol{\omega}_\beta(t); \boldsymbol{\nu}_\beta(t)] = \sum_{i=0}^{n} \mathbf{B}_{i,3}(t)\beta_i, \tag{6}$$

where $\mathbf{B}_{i,3}$ denotes the cubic basis function of B-spline. For more details, please refer to the supplementary material.

3.2 Loss Functions

Building on the continuous representations introduced earlier, in this section, we continue by presenting the differential losses used in our work. Specifically, the differential flow loss Eq. (8) employs the CMax loss [15] to learn optical flow. Additionally, a differential geometric loss is proposed in Eq. (9) to handle the 6-dof motion scenario. By combining these two losses, we are able to overcome the ill-posed problem while simultaneously avoiding the need for depth estimation.

Differential Flow Loss For the differential flow loss, we follow the standard contrast maximization pipeline [15] to learn the continuous optical flow field. Given a set of events input $\mathcal{E} = \{e_k\}_{k=1}^N, e_k \doteq \{\mathbf{x}_k, t_k\}$ with size N, following the definition of warping trajectory defined in Eq. (3), we can warp each of them to a reference time t_{ref}, denoted as $\mathcal{E}(t_{\text{ref}}) = \{e_k(t_{\text{ref}})\}_{k=1}^N$. Then, all the event are accumulated into an image of warped events (IWE),

$$I(\mathbf{x}, \mathcal{E}(t_{\text{ref}})) = \sum_{k=1}^{N} \mathcal{N}(x; \mathbf{x}_k(t_{\text{ref}}), \sigma^2), \tag{7}$$

where σ defines the gaussian smoothing kernel size. Then, by the following differential flow loss, we can measure the concentration of events.

$$L_{\text{flow}}(\mathcal{E}(t_{\text{ref}}), \theta) = -\frac{1}{HW} \sum_{i=1}^{H} \sum_{j=1}^{W} (I_{ij} - \mu_I)^2, \tag{8}$$

where H, W and $\mu_I = \sum_{i=1}^{H} \sum_{j=1}^{W} I_{ij}$ denotes the hight, width and the mean of IWE, respectively.

Differential Geometric Loss In the multi-view geometry literature, there are two equations connect optical flow and ego-motion: the motion field equation [22] and the epipolar equation [23]. Although not widely known, the differential epipolar equation [23] can theoretically be viewed as the differential forms of the epipolar constraint. Our differential geometric loss is primarily based on this equation. Specifically, the 6-DOF motion differential geometric loss in homogeneous coordinate can be defined to be:

$$L_{\text{geometry}}(t, \mathbf{x}, \theta, \beta) = \left\| \hat{\mathbf{u}}_\theta(t, \mathbf{x})^\top [\boldsymbol{\nu}_\beta(t)]_\times \hat{\mathbf{x}} - \hat{\mathbf{x}}^\top \mathbf{s}_\beta(t) \hat{\mathbf{x}} \right\|_2^2, \tag{9}$$

where $\mathbf{s}_\beta(t) = \frac{1}{2}\left([\boldsymbol{\nu}_\beta(t)]_\times [\boldsymbol{\omega}_\beta(t)]_\times + [\boldsymbol{\omega}_\beta(t)]_\times [\boldsymbol{\nu}_\beta(t)]_\times\right)$, hat $\hat{\cdot}$ denotes the homogeneous coordinate and $[\cdot]_\times$ denotes the skew-symmetric operation.

Remark. As shown in Fig. 3, by jointly estimating these two losses, we can prevent optical flow estimation from getting trapped in local minima, making it possible to solve the inherently ill-posed problem involving translational motion.

3.3 Training Pipeline

After collecting the representations and losses, we are ready to build the unsupervised training pipeline. As shown in Fig. 2, given a sequence of event data $\mathcal{E}$, we use differential flow and differential geometric losses to train the neural network and spline parameters.

$$\min_{\theta, \beta} \mathbb{E}_{t_{\text{ref}}} \left[L_{\text{flow}}(\mathcal{E}_{\text{neigh}}(t_{\text{ref}}), \theta) \right] + \mathbb{E}_{\{\mathbf{x}, t\} \sim \mathcal{E}} \left[L_{\text{geometry}}(t, \mathbf{x}, \theta, \beta) \right], \tag{10}$$

For the differential flow loss, we randomly select a reference time t_{ref} and a set of surrounding events $\mathcal{E}_{\text{neigh}}(t_{\text{ref}})$ around it, then evaluate the differential flow loss $L_{\text{flow}}(\mathcal{E}_{\text{neigh}}(t_{\text{ref}}), \theta)$ and back propagate the gradient using Neural ODE to train the network parameters θ. For the differential geometric loss, we randomly sample some events $e = \{\mathbf{x}, t\} \sim \mathcal{E}$, collect the corresponding optical flow for each event $\text{NN}_\theta(t, \text{x})$ and camera velocity $[\boldsymbol{\omega}_\beta(t); \boldsymbol{\nu}_\beta(t)]$ derived from the spline β at time t, compute and accumulate the differential geometric loss, and then back propagate the gradient to train both the neural network θ and the spline β. These two losses are optimized simultaneously until convergence.

4 Experiments

4.1 Experimental Setup

Datasets and Metrics. We conduct comprehensive evaluations on the MVSEC dataset [64], which is the de facto standard dataset used in prior work to benchmark optical flow and 6-DoF ego-motion estimations. This dataset contains both indoor sequences recorded by drones and outdoor sequences recorded by vehicles. Additionally, we benchmarked optical flow estimation on the more challenging DSEC [65] dataset, which features complex textures, diverse motion patterns, and varying lighting conditions. For optical flow evaluation, we compute three standard metrics: endpoint error (EPE), angular error (AE) and the percentage of pixels with EPE > 3 pixels (denoted by "% Out"), exclusively over valid ground truth regions with event activity in the evaluation interval. For motion estimation accuracy, we adopt the root mean square error (RMSE) metric proposed in [14] to measure angular velocity ($^\circ/s$) and linear velocity (m/s) errors.

Baselines. Optical flow estimation using event camera is a widely explored task with various methodological paradigms. We categorize existing approaches into four primary classes: Supervised Learning(SL), which requires ground truch optical flow for training (e.g., E-RAFT [26], EV-FlowNet-EST [25], EV-FlowNet+ [29], DCEIFlow [59], TMA [24], ADM-Flow [31]); Semi-Supervised Learning (SSL), leveraging grayscale images as supervision through photometric loss construction (e.g., EV-FlowNet [18], STE-FlowNet [33]); Unsupervised Learning (USL), relying solely on event data by warping events to reference time and maximizing accumulated image contrast (e.g., MotionPriorCMax [36], ConvGRU-EV-FlowNet [32], FireFlowNet [27], USL-EV-FlowNet [19], ET-FlowNeT [35], EV-MGRFlowNet [63], Paredes *et al.* [37]); and Model-Based (MB) methods, which also adopt contrast maximization objectives but employ traditional nonlinear optimization instead of neural networks (e.g., MultiCM-V2[16], MultiCM [17], Akolkar *et al.* [13], Nagata *et al.* [60], Brebion *et al.* [61], Cuadrado *et al.* [28], Shiba *et al.* [62]). From these paradigms, we select representative prior works as strong baselines for comprehensive quantitative benchmarking of optical flow estimation performance.

Table 1: **Quantitative comparison of optical flow estimation task on MVSEC dataset.** Bold is the best among all methods; underlined is second best. Pink represents the best in the 'USL'; Orange represents the second best in the 'USL'.

		indoor_flying1		indoor_flying2		indoor_flying3		outdoor_day1		average	
	$dt = 1$	EPE ↓	%Out ↓	EPE ↓	%Out ↓	EPE ↓	%Out ↓	EPE ↓	%Out ↓	EPE ↓	%Out ↓
SL	EV-FlowNet-EST [25]	0.97	0.91	1.38	8.20	1.43	6.47	–	–	–	–
SL	EV-FlowNet+ [29]	0.56	1.00	0.66	1.00	0.59	1.00	0.68	0.99	0.623	0.998
SL	E-RAFT [26]	1.10	5.72	1.94	30.79	1.66	25.20	0.24	1.70	1.235	15.853
SL	DCEIFlow [59]	0.75	1.55	0.90	2.10	0.80	1.77	**0.22**	**0.00**	0.668	1.355
SL	TMA [24]	1.06	3.63	1.81	27.29	1.58	23.26	0.25	0.07	1.175	13.563
SL	ADM-Flow [31]	0.52	0.14	0.68	1.18	0.52	0.04	0.41	**0.00**	0.533	0.340
SSL	EV-FlowNet [18]	1.03	2.20	1.72	15.10	1.53	11.90	0.49	0.20	1.193	7.350
SSL	STE-FlowNet [33]	0.57	0.10	0.79	1.60	0.72	1.30	0.42	**0.00**	0.625	0.750
MB	Akolkar *et al.* [13]	1.52	–	1.59	–	1.89	–	2.75	–	1.938	–
MB	Nagata *et al.* [60]	0.62	–	0.93	–	0.84	–	0.77	–	0.790	–
MB	Brebion *et al.* [61]	0.52	0.10	0.98	5.50	0.71	2.10	0.53	0.20	0.685	1.975
MB	Cuadrado *et al.* [28]	0.58	–	0.72	–	0.67	–	0.85	–	0.705	–
MB	Shiba *et al.* [62]	1.05	2.90	1.68	13.44	1.43	8.97	0.94	3.08	1.275	7.098
MB	MultiCM [17]	0.42	0.09	0.60	0.59	0.50	0.29	0.30	0.11	0.455	0.270
MB	MultiCM-V2 [16]	**0.30**	**0.00**	**0.47**	**0.01**	**0.34**	**0.00**	0.28	0.21	**0.348**	**0.055**
USL	USL-EV-FlowNet [19]	0.58	**0.00**	1.02	4.00	0.87	3.00	0.32	**0.00**	0.698	1.750
USL	FireFlowNet [27]	0.97	2.60	1.67	15.30	1.43	11.00	1.06	6.60	1.283	8.875
USL	ConvGRU-EV-FlowNet [32]	0.60	0.51	1.17	8.06	0.93	5.64	0.47	0.25	0.793	3.615
USL	ET-FlowNeT [35]	0.57	0.53	1.20	8.48	0.95	5.73	0.39	0.12	0.778	3.715
USL	EV-MGRFlowNet [63]	0.41	0.17	0.70	2.35	0.59	1.29	0.28	0.02	0.495	0.958
USL	Paredes *et al.* [37]	0.44	**0.00**	0.88	4.51	0.70	2.41	0.27	0.05	0.573	1.743
USL	MotionPriorCMax [36]	0.45	0.09	0.71	2.40	0.60	0.93	–	–	–	–
USL	Ours	0.40	0.30	0.52	0.18	0.46	0.29	0.42	0.54	0.450	0.328
	$dt = 4$										
SL	E-RAFT [26]	2.81	40.25	5.09	64.19	4.46	57.11	0.72	1.12	3.270	40.668
SL	DCEIFlow [59]	2.08	21.47	3.48	42.05	2.51	29.73	0.89	3.19	2.240	24.110
SL	TMA [24]	2.43	29.91	4.32	52.74	3.60	42.02	**0.70**	**1.08**	2.762	31.438
SL	ADM-Flow [31]	1.42	7.78	1.88	16.70	1.61	11.40	1.51	10.20	1.605	11.520
SSL	EV-FlowNet [18]	2.25	24.70	4.05	45.30	3.45	39.70	1.23	7.30	2.745	29.250
SSL	STE-FlowNet [33]	1.77	14.70	2.52	26.10	2.23	22.10	0.99	3.90	1.878	16.700
MB	Shiba *et al.* [62]	4.06	53.88	6.39	71.82	5.36	65.57	3.60	49.04	4.853	60.077
MB	MultiCM [17]	1.68	12.79	2.49	26.31	2.06	18.93	1.25	9.19	1.870	16.805
MB	MultiCM-V2 [16]	**1.18**	**4.77**	**1.87**	**15.51**	**1.38**	**7.62**	1.05	5.68	**1.108**	**8.305**
USL	USL-EV-FlowNet [19]	2.18	24.20	3.85	46.80	3.18	47.80	1.30	9.70	2.628	32.125
USL	ConvGRU-EV-FlowNet [32]	2.16	21.51	3.90	40.72	3.00	29.60	1.69	12.50	2.688	26.083
USL	ET-FlowNeT [35]	2.08	20.02	3.99	41.33	3.13	31.70	1.47	9.17	2.667	25.555
USL	EV-MGRFlowNet [63]	1.50	8.67	2.39	23.70	2.06	18.00	1.10	6.22	1.763	14.147
USL	Ours	1.58	9.2	2.04	18.54	1.84	13.57	1.63	14.42	1.773	13.933

For 6-DoF motion estimation, existing methods can be categorized into two classes based on whether depth prior knowledge is required. Approaches such as AEmin [42], Incmin [66], and PEME [43] require depth-augmented event data to achieve a 6-DoF estimation, while ECN [48] and MultiCM-V2 [16] can perform a 6-DoF estimation relying solely on raw event streams without depth priors.

Implementation Details. The neural implicit flow field adopts the MLP architecture. The detailed network architecture can be found in appendix. Following prior works [17] [43], we partition the entire event sequence into multiple segments during training, with each segment containing 30k events for MVSEC [64] and 300k events for DSEC [65]. Because the time interval of each segment is short, the cubic spline modeling continuous camera motion employs only 4 control knots, whose 6-dimensional vectors are initialized to a constant value of 0.2. To solve the event warping trajectory Eq. (2), we employ the euler solver for its computational efficiency in numerical integration. The weight of the differential geometric loss is set to 0.25 and the differential flow loss to 1. We employ two separate AdamW optimizers [67] for the neural implicit flow field NN_θ and the camera motion parameters β. For the MVSEC dataset, the learning rate for the flow field is exponentially decayed from 1×10^{-4} to 6.3×10^{-5}, whereas for the DSEC dataset, it is cosine annealed from 2×10^{-3}

Table 2: **Quantitative comparison of optical flow estimation task on DSEC dataset.** Bold is the best among all methods; underlined is second best. Pink represents the best in the 'USL'; Orange represents the second best in the 'USL'.

	All			interlaken_00_b			interlaken_01_a			thun_01_a		
Method	EPE ↓	AE ↓	%Out ↓	EPE ↓	AE ↓	%Out ↓	EPE ↓	AE ↓	%Out ↓	EPE ↓	AE ↓	%Out ↓
(SL) E-RAFT [26]	0.79	2.85	2.68	**1.39**	2.36	6.19	0.90	2.54	3.91	0.65	2.94	1.87
(SL) TMA [24]	**0.74**	**2.68**	**2.30**	**1.39**	**2.16**	**5.79**	**0.81**	**2.23**	**3.11**	**0.62**	**2.88**	**1.61**
(MB) MultiCM-V2 [16]	3.47	13.98	30.86	5.74	9.19	38.93	3.74	9.77	31.37	2.12	11.06	17.68
(USL) Paredes et al. [37]	2.33	10.56	17.77	3.34	6.22	25.72	2.49	6.88	19.15	1.73	9.75	10.39
(USL) MotionPriorCMax [36]	3.20	8.53	15.21	3.21	4.89	20.45	2.38	5.46	17.40	1.39	6.99	7.36
(USL) EV-FlowNet [19]	3.86	–	31.45	6.32	–	47.95	4.91	–	36.07	2.33	–	20.92
(USL) Ours	3.14	10.87	19.43	7.24	14.43	35.53	3.18	7.52	19.21	1.83	6.89	12.65

	thun_01_b			zurich_city_12_a			zurich_city_14_c			zurich_city_15_a		
Method	EPE ↓	AE ↓	%Out ↓	EPE ↓	AE ↓	%Out ↓	EPE ↓	AE ↓	%Out ↓	EPE ↓	AE ↓	%Out ↓
(SL) E-RAFT [26]	0.58	2.20	1.52	0.61	4.50	1.06	0.71	3.43	**1.91**	0.59	2.55	1.30
(SL) TMA [24]	**0.55**	**2.10**	**1.31**	**0.57**	**4.38**	**0.87**	**0.66**	**3.09**	1.99	**0.55**	**2.51**	**1.08**
(MB) MultiCM-V2 [17]	2.48	12.05	23.56	3.86	28.61	43.96	2.72	12.62	30.53	2.35	11.82	20.99
(USL) Paredes et al. [37]	1.66	8.41	9.34	2.72	23.16	26.65	2.64	10.23	23.01	1.69	8.88	9.98
(USL) MotionPriorCMax [36]	1.54	6.55	9.69	8.33	20.16	22.39	1.78	8.79	12.99	1.45	6.27	8.34
(USL) EV-FlowNet [19]	3.04	–	25.41	2.62	–	25.80	3.36	–	36.34	2.97	–	25.53
(USL) Ours	1.66	5.62	10.55	3.52	24.92	28.51	1.89	6.13	15.44	1.51	5.66	9.08

Table 3: **Quantitative comparison of 6-DoF egomotion estimation task on MVSEC dataset.** The notation "w/ *D*" denotes requiring depth prior information, whereas "w/o *D*" indicates no need for depth information. Bold is the best among all methods; underlined is second best.

		indoor_flying1		indoor_flying2		indoor_flying3		outdoor_day1		average	
		RMS_ω↓	RMS_v↓	RMS_ω↓	RMS_v↓	RMS_ω↓	RMS_v↓	RMS_ω↓	RMS_v↓	RMS_ω↓	RMS_v↓
w/ *D*	AEmin [42]	1.38	0.069	–	–	–	–	4.00	0.677	–	–
	IncEmin [66]	1.65	0.085	–	–	–	–	4.05	1.035	–	–
	PEME [43]	**1.05**	**0.039**	–	–	–	–	2.72	0.598	–	–
w/o *D*	ECN [48]	–	–	–	–	–	–	–	0.70	–	–
	MultiCM-V2 [16]	7.72	0.24	11.50	0.27	9.53	0.31	6.85	5.90	8.900	1.680
	Ours	3.44	0.11	**5.31**	**0.12**	**4.12**	**0.15**	**3.38**	**0.76**	**4.062**	**0.285**

to 1×10^{-7}. The learning rate for the camera motion is kept constant at 1×10^{-3} for both datasets. Each short event segment is trained for 1k iterations. All experiments were conducted on a NVIDIA RTX 4090.

4.2 Results on Optical Flow Estimation

Quantitative Results. We conduct comprehensive quantitative benchmarking for optical flow estimation on the MVSEC dataset [64] and DSEC dataset [68], as detailed in Tab. 1 and Tab. 2. The MVSEC benchmarks optical flow estimation over one-frame ($dt = 1$) and four-frame ($dt = 4$) intervals, respectively. Our method outperforms all existing unsupervised learning methods on the MVSEC dataset. Notably, under the $dt = 1$ setting, our method ranks second among all methods, only behind the traditional optimization-based method MultiCM-V2 [16], and outperforms all supervised learning methods. On the DSEC benchmark, our method performs comparably to existing unsupervised learning approaches. However, there remains a performance gap compared to supervised methods. This is primarily because driving scenes involve more complex motion patterns, abrupt illumination changes, and unstructured scene depth, all of which make it more challenging for unsupervised methods to learn accurate optical flow. The experimental results demonstrate that by introducing implicit spatial-temporal continuity constraints Eq. (2) and differential geometric constraints Eq. (9), our method can unlock the network's representation capacity in an unsupervised learning manner, thereby predicting more accurate optical flow.

Qualitative Results. We performed a qualitative comparison with strong baselines on the MVSEC dataset and DSEC datasets. As shown in Fig.5, the results on the MVSEC datsets demonstrate that our method predicts optical flow closer to the ground truth. Fig. 6 illustrates that our method also

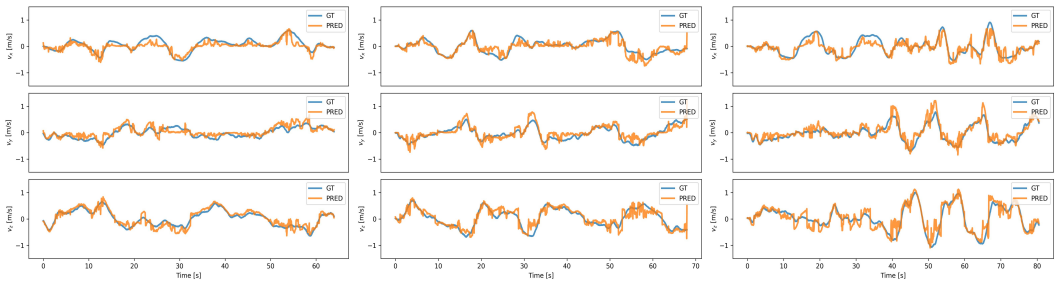

Figure 4: **Qualitative results of 6-DoF motion estimation on the MVSEC dataset.** Due to space constraints, this figure only presents the linear velocity estimation results. The angular velocity results are provided in the supplementary material. The top, middle, and bottom rows in each subfigure correspond to the x-axis, y-axis, and z-axis results, respectively.

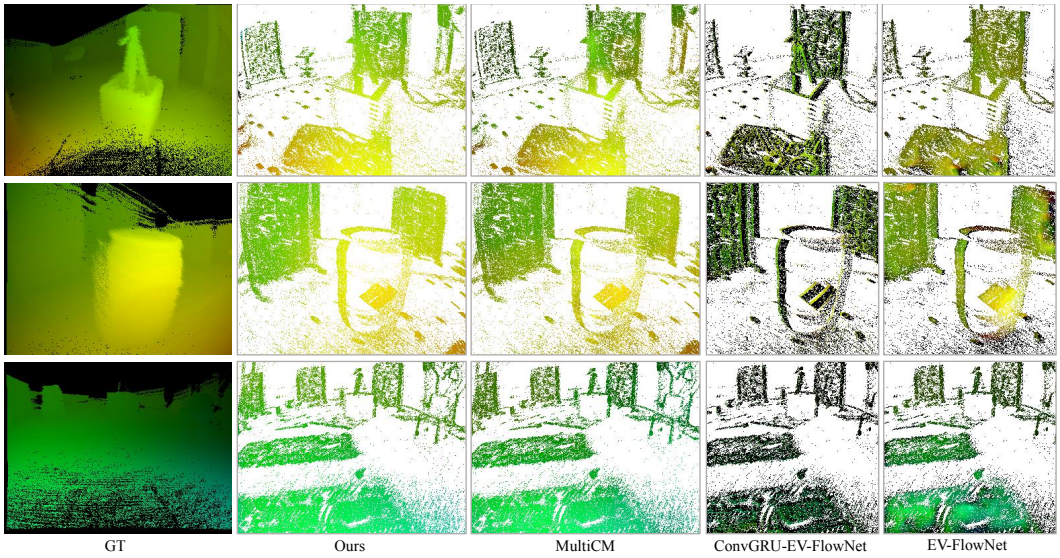

Figure 5: **Qualitative results of optical flow estimation on the MVSEC dataset.** The results in the first, second, and third rows correspond to sequences *indoor_flying1*, *indoor_flying2* and *indoor_flying3*, respectively.

achieved good performance on the DSEC dataset and features smooth optical flow visualizations. Note that we visualize optical flow only at pixels where events are triggered.

4.3 Results on 6-DoF EgoMotion Estimation

Quantitative Results. To evaluate the performance of 6-DoF motion estimation, we compared our method with existing approaches on the MVSEC dataset [64], as it provides ground truth camera motion including angular and linear velocities. As shown in Tab. 3, our method achieves state-of-the-art 6-DoF motion estimation performance in both indoor and outdoor scenes. This is primarily attributed to our method's use of splines to represent camera motion Eq. (6), which provides a strong continuity prior, combined with our designed differential geometric loss Eq. (9). This loss enables optical flow information to offer geometrically meaningful guidance for motion learning without requiring depth priors.

Qualitative Results. We also conducted qualitative evaluation on the 6-DoF motion estimation. As illustrated in Fig. 4, the 6-DoF motion estimated by our method closely matches the ground truth, demonstrating that our approach can achieve outstanding motion estimation performance without requiring depth information in an unsupervised paradigm.

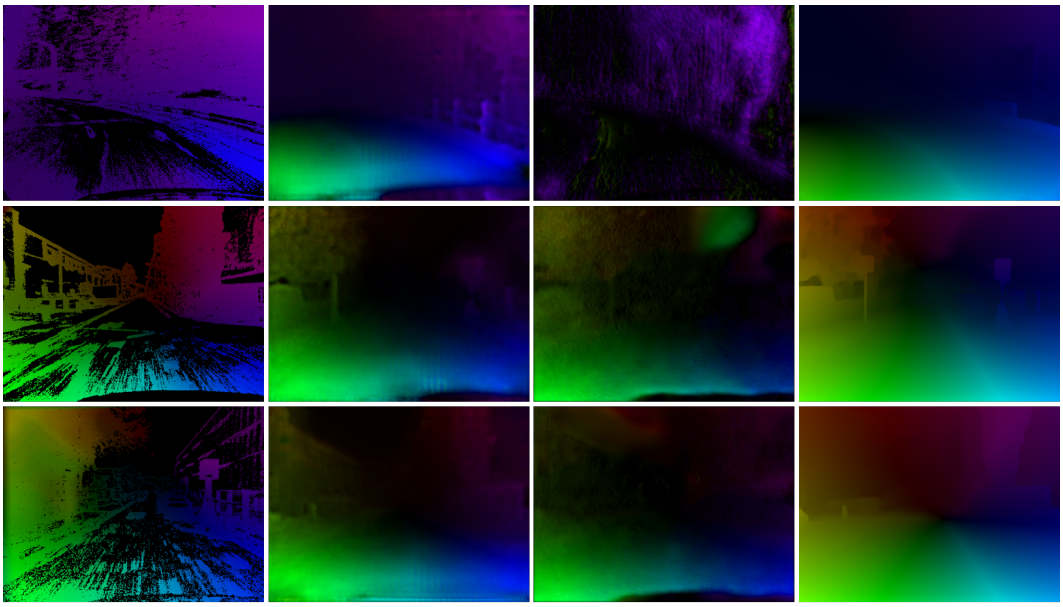

Figure 6: **Qualitative results of optical flow estimation on the DSEC dataset.** The results in the first, second, and third rows correspond to sequences *zurich_city_15a*, *zurich_city_14c* and *interlaken_01a*, respectively.

Table 4: **Ablation studies on differential geometric constraints.**

	indoor_flying1		indoor_flying2		indoor_flying3		outdoor_day1	
$dt = 4$	EPE ↓	%Out ↓	EPE ↓	%Out ↓	EPE ↓	%Out ↓	EPE ↓	%Out ↓
w/o geometric constrain	1.84	9.68	2.27	18.76	2.27	13.72	1.67	15.13
w/ geometric constrain	1.58	9.2	2.04	18.54	1.84	13.57	1.63	14.42
ground truth motion	1.56	9.13	2.04	18.43	1.84	13.57	1.61	14.25

4.4 Ablation Study

To validate the efficacy of differential geometric constraints Eq. (9), we conducted ablation studies on the MVSEC dataset [64] under $dt = 4$ with three configurations: *a)* no geometric constraints, *b)* with differential geometric constraints, and *c)* direct supervised by ground truth motion. As demonstrated in Tab. 4, the differential geometric constraints yield improvements in optical flow estimation, even achieving performance comparable to those supervised with ground truth motion on *indoor_flying2* and *indoor_flying3*. This indicates that our design enhances the geometric plausibility of the estimated optical flow while effectively avoiding convergence to local minima, as visualized in Fig. 3.

5 Conclusion

This work presents **E-MoFlow**, a novel framework that unifies 6-DoF egomotion and optical flow estimation using implicit spatial-temporal and geometric regularization within an unsupervised learning paradigm. By incorporating implicit neural representations with differential geometry constraints, our approach effectively tackles the ill-posed challenges of separate estimations of flow and egomotion from event data. Extensive experiments demonstrate that **E-MoFlow** achieves state-of-the-art performance across diverse motion scenarios, matching or surpassing many supervised approaches.

Acknowledgements. This work was supported in part by NSFC under Grant 62202389, in part by a grant from the Westlake University-Muyuan Joint Research Institute, and in part by the Westlake Education Foundation.

References

[1] Steven S. Beauchemin and John L. Barron. The computation of optical flow. ACM computing surveys (CSUR), 27(3):433–466, 1995.

[2] Richard Hartley. Multiple view geometry in computer vision, volume 665. Cambridge university press, 2003.

[3] Alper Yilmaz, Omar Javed, and Mubarak Shah. Object tracking: A survey. Acm computing surveys (CSUR), 38(4):13–es, 2006.

[4] Wenhan Luo, Junliang Xing, Anton Milan, Xiaoqin Zhang, Wei Liu, and Tae-Kyun Kim. Multiple object tracking: A literature review. Artificial intelligence, 293:103448, 2021.

[5] Linfei Pan, Dániel Baráth, Marc Pollefeys, and Johannes L Schönberger. Global structure-from-motion revisited. In European Conference on Computer Vision, pages 58–77. Springer, 2024.

[6] Johannes L Schonberger and Jan-Michael Frahm. Structure-from-motion revisited. In Proceedings of the IEEE conference on computer vision and pattern recognition, pages 4104–4113, 2016.

[7] Carlos Campos, Richard Elvira, Juan J Gómez Rodríguez, José MM Montiel, and Juan D Tardós. Orb-slam3: An accurate open-source library for visual, visual–inertial, and multimap slam. IEEE transactions on robotics, 37(6):1874–1890, 2021.

[8] Jakob Engel, Vladlen Koltun, and Daniel Cremers. Direct sparse odometry. IEEE transactions on pattern analysis and machine intelligence, 40(3):611–625, 2017.

[9] Jakob Engel, Thomas Schöps, and Daniel Cremers. Lsd-slam: Large-scale direct monocular slam. In European conference on computer vision, pages 834–849. Springer, 2014.

[10] Luo Juan and Oubong Gwun. A comparison of sift, pca-sift and surf. International Journal of Image Processing (IJIP), 3(4):143–152, 2009.

[11] Jean-Yves Bouguet et al. Pyramidal implementation of the affine lucas kanade feature tracker description of the algorithm. Intel corporation, 5(1-10):4, 2001.

[12] Guillermo Gallego, Tobi Delbrück, Garrick Orchard, Chiara Bartolozzi, Brian Taba, Andrea Censi, Stefan Leutenegger, Andrew J Davison, Jörg Conradt, Kostas Daniilidis, et al. Event-based vision: A survey. IEEE transactions on pattern analysis and machine intelligence, 44(1):154–180, 2020.

[13] Himanshu Akolkar, Sio-Hoi Ieng, and Ryad Benosman. Real-time high speed motion prediction using fast aperture-robust event-driven visual flow. IEEE Transactions on Pattern Analysis and Machine Intelligence, 44(1):361–372, 2020.

[14] Zhongyang Ren, Bangyan Liao, Delei Kong, Jinghang Li, Peidong Liu, Laurent Kneip, Guillermo Gallego, and Yi Zhou. Motion and structure from event-based normal flow. In European Conference on Computer Vision, pages 108–125. Springer, 2024.

[15] Guillermo Gallego, Henri Rebecq, and Davide Scaramuzza. A unifying contrast maximization framework for event cameras, with applications to motion, depth, and optical flow estimation. In Proceedings of the IEEE conference on computer vision and pattern recognition, pages 3867–3876, 2018.

[16] Shintaro Shiba, Yannick Klose, Yoshimitsu Aoki, and Guillermo Gallego. Secrets of event-based optical flow, depth and ego-motion estimation by contrast maximization. IEEE Transactions on Pattern Analysis and Machine Intelligence, 2024.

[17] Shintaro Shiba, Yoshimitsu Aoki, and Guillermo Gallego. Secrets of event-based optical flow. In European Conference on Computer Vision, pages 628–645. Springer, 2022.

[18] Alex Zhu, Liangzhe Yuan, Kenneth Chaney, and Kostas Daniilidis. Ev-flownet: Self-supervised optical flow estimation for event-based cameras. In Proceedings of Robotics: Science and Systems, Pittsburgh, Pennsylvania, June 2018.

[19] Alex Zihao Zhu, Liangzhe Yuan, Kenneth Chaney, and Kostas Daniilidis. Unsupervised event-based learning of optical flow, depth, and egomotion. In Proceedings of the IEEE/CVF conference on computer vision and pattern recognition, pages 989–997, 2019.

[20] Larry Schumaker. Spline functions: basic theory. Cambridge university press, 2007.

[21] Vincent Sitzmann, Julien Martel, Alexander Bergman, David Lindell, and Gordon Wetzstein. Implicit neural representations with periodic activation functions. Advances in neural information processing systems, 33:7462–7473, 2020.

[22] Hugh Christopher Longuet-Higgins and Kvetoslav Prazdny. The interpretation of a moving retinal image. Proceedings of the Royal Society of London. Series B. Biological Sciences, 208(1173):385–397, 1980.

[23] Yi Ma, Stefano Soatto, Jana Košecká, and Shankar Sastry. An invitation to 3-d vision: from images to geometric models, volume 26. Springer, 2004.

[24] Haotian Liu, Guang Chen, Sanqing Qu, Yanping Zhang, Zhijun Li, Alois Knoll, and Changjun Jiang. Tma: Temporal motion aggregation for event-based optical flow. In Proceedings of the IEEE/CVF International Conference on Computer Vision, pages 9685–9694, 2023.

[25] Daniel Gehrig, Antonio Loquercio, Konstantinos G Derpanis, and Davide Scaramuzza. End-to-end learning of representations for asynchronous event-based data. In Proceedings of the IEEE/CVF International Conference on Computer Vision, pages 5633–5643, 2019.

[26] Mathias Gehrig, Mario Millhäusler, Daniel Gehrig, and Davide Scaramuzza. E-raft: Dense optical flow from event cameras. In 2021 International Conference on 3D Vision (3DV), pages 197–206. IEEE, 2021.

[27] Federico Paredes-Vallés and Guido CHE De Croon. Back to event basics: Self-supervised learning of image reconstruction for event cameras via photometric constancy. In Proceedings of the IEEE/CVF Conference on Computer Vision and Pattern Recognition, pages 3446–3455, 2021.

[28] Javier Cuadrado, Ulysse Rançon, Benoit R Cottereau, Francisco Barranco, and Timothée Masquelier. Optical flow estimation from event-based cameras and spiking neural networks. Frontiers in Neuroscience, 17:1160034, 2023.

[29] Timo Stoffregen, Cedric Scheerlinck, Davide Scaramuzza, Tom Drummond, Nick Barnes, Lindsay Kleeman, and Robert Mahony. Reducing the sim-to-real gap for event cameras. In Computer Vision–ECCV 2020: 16th European Conference, Glasgow, UK, August 23–28, 2020, Proceedings, Part XXVII 16, pages 534–549. Springer, 2020.

[30] Mathias Gehrig, Manasi Muglikar, and Davide Scaramuzza. Dense continuous-time optical flow from event cameras. IEEE Transactions on Pattern Analysis and Machine Intelligence, 46(7):4736–4746, 2024.

[31] Xinglong Luo, Kunming Luo, Ao Luo, Zhengning Wang, Ping Tan, and Shuaicheng Liu. Learning optical flow from event camera with rendered dataset. In Proceedings of the IEEE/CVF International Conference on Computer Vision, pages 9847–9857, 2023.

[32] Jesse Hagenaars, Federico Paredes-Vallés, and Guido De Croon. Self-supervised learning of event-based optical flow with spiking neural networks. Advances in Neural Information Processing Systems, 34:7167–7179, 2021.

[33] Ziluo Ding, Rui Zhao, Jiyuan Zhang, Tianxiao Gao, Ruiqin Xiong, Zhaofei Yu, and Tiejun Huang. Spatio-temporal recurrent networks for event-based optical flow estimation. In Proceedings of the AAAI conDference on artificial intelligence, volume 36, pages 525–533, 2022.

[34] Chankyu Lee, Adarsh Kumar Kosta, Alex Zihao Zhu, Kenneth Chaney, Kostas Daniilidis, and Kaushik Roy. Spike-flownet: event-based optical flow estimation with energy-efficient hybrid neural networks. In European Conference on Computer Vision, pages 366–382. Springer, 2020.

[35] Yi Tian and Juan Andrade-Cetto. Event transformer flownet for optical flow estimation. 2022.

[36] Friedhelm Hamann, Ziyun Wang, Ioannis Asmanis, Kenneth Chaney, Guillermo Gallego, and Kostas Daniilidis. Motion-prior contrast maximization for dense continuous-time motion estimation. In European Conference on Computer Vision, pages 18–37. Springer, 2024.

[37] Federico Paredes-Vallés, Kirk YW Scheper, Christophe De Wagter, and Guido CHE De Croon. Taming contrast maximization for learning sequential, low-latency, event-based optical flow. In Proceedings of the IEEE/CVF International Conference on Computer Vision, pages 9695–9705, 2023.

[38] Ling Gao, Hang Su, Daniel Gehrig, Marco Cannici, Davide Scaramuzza, and Laurent Kneip. A 5-point minimal solver for event camera relative motion estimation. In Proceedings of the IEEE/CVF International Conference on Computer Vision, pages 8049–8059, 2023.

[39] Ling Gao, Daniel Gehrig, Hang Su, Davide Scaramuzza, and Laurent Kneip. An n-point linear solver for line and motion estimation with event cameras. In Proceedings of the IEEE/CVF Conference on Computer Vision and Pattern Recognition, pages 14596–14605, 2024.

[40] Guillermo Gallego, Mathias Gehrig, and Davide Scaramuzza. Focus is all you need: Loss functions for event-based vision. In Proceedings of the IEEE/CVF Conference on Computer Vision and Pattern Recognition, pages 12280–12289, 2019.

[41] Shintaro Shiba, Yoshimitsu Aoki, and Guillermo Gallego. Event collapse in contrast maximization frameworks. Sensors, 22(14):5190, 2022.

[42] Urbano Miguel Nunes and Yiannis Demiris. Entropy minimisation framework for event-based vision model estimation. In Computer Vision–ECCV 2020: 16th European Conference, Glasgow, UK, August 23–28, 2020, Proceedings, Part V 16, pages 161–176. Springer, 2020.

[43] Xueyan Huang, Yueyi Zhang, and Zhiwei Xiong. Progressive spatio-temporal alignment for efficient event-based motion estimation. In Proceedings of the IEEE/CVF Conference on Computer Vision and Pattern Recognition, pages 1537–1546, 2023.

[44] Jinghang Li, Bangyan Liao, Xiuyuan Lu, Peidong Liu, Shaojie Shen, and Yi Zhou. Event-aided time-to-collision estimation for autonomous driving. In European Conference on Computer Vision, pages 57–73. Springer, 2024.

[45] Daqi Liu, Alvaro Parra, and Tat-Jun Chin. Spatiotemporal registration for event-based visual odometry. In Proceedings of the IEEE/CVF conference on computer vision and pattern recognition, pages 4937–4946, 2021.

[46] Yi Zhou, Guillermo Gallego, and Shaojie Shen. Event-based stereo visual odometry. IEEE Transactions on Robotics, 37(5):1433–1450, 2021.

[47] Ji Zhao, Banglei Guan, Zibin Liu, and Laurent Kneip. Full-dof egomotion estimation for event cameras using geometric solvers. arXiv preprint arXiv:2503.03307, 2025.

[48] Chengxi Ye, Anton Mitrokhin, Cornelia Fermüller, James A Yorke, and Yiannis Aloimonos. Unsupervised learning of dense optical flow, depth and egomotion with event-based sensors. In 2020 IEEE/RSJ International Conference on Intelligent Robots and Systems (IROS), pages 5831–5838. IEEE, 2020.

[49] Matthew Tancik, Pratul Srinivasan, Ben Mildenhall, Sara Fridovich-Keil, Nithin Raghavan, Utkarsh Singhal, Ravi Ramamoorthi, Jonathan Barron, and Ren Ng. Fourier features let networks learn high frequency functions in low dimensional domains. Advances in neural information processing systems, 33:7537–7547, 2020.

[50] Ben Mildenhall, Pratul P Srinivasan, Matthew Tancik, Jonathan T Barron, Ravi Ramamoorthi, and Ren Ng. Nerf: Representing scenes as neural radiance fields for view synthesis. Communications of the ACM, 65(1):99–106, 2021.

[51] Wenpu Li, Pian Wan, Peng Wang, Jinghang Li, Yi Zhou, and Peidong Liu. Benerf: neural radiance fields from a single blurry image and event stream. In European Conference on Computer Vision, pages 416–434. Springer, 2024.

[52] Kyle Vedder, Neehar Peri, Ishan Khatri, Siyi Li, Eric Eaton, Mehmet Kocamaz, Yue Wang, Zhiding Yu, Deva Ramanan, and Joachim Pehserl. Neural eulerian scene flow fields. arXiv preprint arXiv:2410.02031, 2024.

[53] Xueqian Li, Jhony Kaesemodel Pontes, and Simon Lucey. Neural scene flow prior. Advances in Neural Information Processing Systems, 34:7838–7851, 2021.

[54] Chaoyang Wang, Xueqian Li, Jhony Kaesemodel Pontes, and Simon Lucey. Neural prior for trajectory estimation. In Proceedings of the IEEE/CVF Conference on Computer Vision and Pattern Recognition, pages 6532–6542, 2022.

[55] Ricky TQ Chen, Yulia Rubanova, Jesse Bettencourt, and David K Duvenaud. Neural ordinary differential equations. Advances in neural information processing systems, 31, 2018.

[56] B.N. Biswas, Somnath Chatterjee, SP Mukherjee, and Subhradeep Pal. A discussion on euler method: A review. Electronic Journal of Mathematical Analysis and Applications, 1(2):2090–2792, 2013.

[57] John Charles Butcher. A history of runge-kutta methods. Applied numerical mathematics, 20(3):247–260, 1996.

[58] Lawrence F Shampine. Some practical runge-kutta formulas. Mathematics of computation, 46(173):135–150, 1986.

[59] Zhexiong Wan, Yuchao Dai, and Yuxin Mao. Learning dense and continuous optical flow from an event camera. IEEE Transactions on Image Processing, 31:7237–7251, 2022.

[60] Jun Nagata, Yusuke Sekikawa, and Yoshimitsu Aoki. Optical flow estimation by matching time surface with event-based cameras. Sensors, 21(4), 2021.

[61] Vincent Brebion, Julien Moreau, and Franck Davoine. Real-time optical flow for vehicular perception with low- and high-resolution event cameras. IEEE Transactions on Intelligent Transportation Systems, 23(9):15066–15078, 2022.

[62] Shintaro Shiba, Yoshimitsu Aoki, and Guillermo Gallego. Fast event-based optical flow estimation by triplet matching. IEEE Signal Processing Letters, 29:2712–2716, 2022.

[63] Hao Zhuang, Zheng Fang, Xinjie Huang, Kuanxu Hou, Delei Kong, and Chenming Hu. Ev-mgrflownet: Motion-guided recurrent network for unsupervised event-based optical flow with hybrid motion-compensation loss. IEEE Transactions on Instrumentation and Measurement, 73:1–15, 2024.

[64] Alex Zihao Zhu, Dinesh Thakur, Tolga Özaslan, Bernd Pfrommer, Vijay Kumar, and Kostas Daniilidis. The multivehicle stereo event camera dataset: An event camera dataset for 3d perception. IEEE Robotics and Automation Letters, 3(3):2032–2039, 2018.

[65] Mathias Gehrig, Willem Aarents, Daniel Gehrig, and Davide Scaramuzza. Dsec: A stereo event camera dataset for driving scenarios. IEEE Robotics and Automation Letters, 2021.

[66] Urbano Miguel Nunes and Yiannis Demiris. Robust event-based vision model estimation by dispersion minimisation. IEEE Transactions on Pattern Analysis and Machine Intelligence, 44(12):9561–9573, 2022.

[67] Ilya Loshchilov and Frank Hutter. Decoupled weight decay regularization. In International Conference on Learning Representations.

[68] Mathias Gehrig, Willem Aarents, Daniel Gehrig, and Davide Scaramuzza. Dsec: A stereo event camera dataset for driving scenarios. IEEE Robotics and Automation Letters, 2021.

[69] Ben Mildenhall, Pratul P. Srinivasan, Matthew Tancik, Jonathan T. Barron, Ravi Ramamoorthi, and Ren Ng. Nerf: Representing scenes as neural radiance fields for view synthesis. In ECCV, 2020.

[70] Matt Jordan and Alexandros G Dimakis. Exactly computing the local lipschitz constant of relu networks. Advances in Neural Information Processing Systems, 33:7344–7353, 2020.

[71] Aladin Virmaux and Kevin Scaman. Lipschitz regularity of deep neural networks: analysis and efficient estimation. Advances in Neural Information Processing Systems, 31, 2018.

[72] Nasim Rahaman, Aristide Baratin, Devansh Arpit, Felix Draxler, Min Lin, Fred Hamprecht, Yoshua Bengio, and Aaron Courville. On the spectral bias of neural networks. In Kamalika Chaudhuri and Ruslan Salakhutdinov, editors, Proceedings of the 36th International Conference on Machine Learning, volume 97 of Proceedings of Machine Learning Research, pages 5301–5310. PMLR, 09–15 Jun 2019.

[73] Marco Zucchelli. Optical flow based structure from motion. PhD thesis, Numerisk analys och datalogi, 2002.

NeurIPS Paper Checklist

1. **Claims**

   Question: Do the main claims made in the abstract and introduction accurately reflect the paper's contributions and scope?

   Answer: [Yes]

   Justification: The abstract and introduction accurately reflect the paper's contributions and scope.

   Guidelines:

   - The answer NA means that the abstract and introduction do not include the claims made in the paper.
   - The abstract and/or introduction should clearly state the claims made, including the contributions made in the paper and important assumptions and limitations. A No or NA answer to this question will not be perceived well by the reviewers.
   - The claims made should match theoretical and experimental results, and reflect how much the results can be expected to generalize to other settings.
   - It is fine to include aspirational goals as motivation as long as it is clear that these goals are not attained by the paper.

2. **Limitations**

   Question: Does the paper discuss the limitations of the work performed by the authors?

   Answer: [Yes]

   Justification: We summarize the limitations of this work in the conclusion.

   Guidelines:

   - The answer NA means that the paper has no limitation while the answer No means that the paper has limitations, but those are not discussed in the paper.
   - The authors are encouraged to create a separate "Limitations" section in their paper.
   - The paper should point out any strong assumptions and how robust the results are to violations of these assumptions (e.g., independence assumptions, noiseless settings, model well-specification, asymptotic approximations only holding locally). The authors should reflect on how these assumptions might be violated in practice and what the implications would be.
   - The authors should reflect on the scope of the claims made, e.g., if the approach was only tested on a few datasets or with a few runs. In general, empirical results often depend on implicit assumptions, which should be articulated.
   - The authors should reflect on the factors that influence the performance of the approach. For example, a facial recognition algorithm may perform poorly when image resolution is low or images are taken in low lighting. Or a speech-to-text system might not be used reliably to provide closed captions for online lectures because it fails to handle technical jargon.
   - The authors should discuss the computational efficiency of the proposed algorithms and how they scale with dataset size.
   - If applicable, the authors should discuss possible limitations of their approach to address problems of privacy and fairness.
   - While the authors might fear that complete honesty about limitations might be used by reviewers as grounds for rejection, a worse outcome might be that reviewers discover limitations that aren't acknowledged in the paper. The authors should use their best judgment and recognize that individual actions in favor of transparency play an important role in developing norms that preserve the integrity of the community. Reviewers will be specifically instructed to not penalize honesty concerning limitations.

3. **Theory assumptions and proofs**

   Question: For each theoretical result, does the paper provide the full set of assumptions and a complete (and correct) proof?

   Answer: [Yes]

Justification: For each important equation in methodology section, we have clearly indicated its source citation.

Guidelines:

- The answer NA means that the paper does not include theoretical results.
- All the theorems, formulas, and proofs in the paper should be numbered and cross-referenced.
- All assumptions should be clearly stated or referenced in the statement of any theorems.
- The proofs can either appear in the main paper or the supplemental material, but if they appear in the supplemental material, the authors are encouraged to provide a short proof sketch to provide intuition.
- Inversely, any informal proof provided in the core of the paper should be complemented by formal proofs provided in appendix or supplemental material.
- Theorems and Lemmas that the proof relies upon should be properly referenced.

4. **Experimental result reproducibility**

   Question: Does the paper fully disclose all the information needed to reproduce the main experimental results of the paper to the extent that it affects the main claims and/or conclusions of the paper (regardless of whether the code and data are provided or not)?

   Answer: [Yes]

   Justification: In the experiments section, we provide a detailed description of our implementation, and we will release the source code upon acceptance.

   Guidelines:

   - The answer NA means that the paper does not include experiments.
   - If the paper includes experiments, a No answer to this question will not be perceived well by the reviewers: Making the paper reproducible is important, regardless of whether the code and data are provided or not.
   - If the contribution is a dataset and/or model, the authors should describe the steps taken to make their results reproducible or verifiable.
   - Depending on the contribution, reproducibility can be accomplished in various ways. For example, if the contribution is a novel architecture, describing the architecture fully might suffice, or if the contribution is a specific model and empirical evaluation, it may be necessary to either make it possible for others to replicate the model with the same dataset, or provide access to the model. In general. releasing code and data is often one good way to accomplish this, but reproducibility can also be provided via detailed instructions for how to replicate the results, access to a hosted model (e.g., in the case of a large language model), releasing of a model checkpoint, or other means that are appropriate to the research performed.
   - While NeurIPS does not require releasing code, the conference does require all submissions to provide some reasonable avenue for reproducibility, which may depend on the nature of the contribution. For example
     (a) If the contribution is primarily a new algorithm, the paper should make it clear how to reproduce that algorithm.
     (b) If the contribution is primarily a new model architecture, the paper should describe the architecture clearly and fully.
     (c) If the contribution is a new model (e.g., a large language model), then there should either be a way to access this model for reproducing the results or a way to reproduce the model (e.g., with an open-source dataset or instructions for how to construct the dataset).
     (d) We recognize that reproducibility may be tricky in some cases, in which case authors are welcome to describe the particular way they provide for reproducibility. In the case of closed-source models, it may be that access to the model is limited in some way (e.g., to registered users), but it should be possible for other researchers to have some path to reproducing or verifying the results.

5. **Open access to data and code**

Question: Does the paper provide open access to the data and code, with sufficient instructions to faithfully reproduce the main experimental results, as described in supplemental material?

Answer: [No]

Justification: We will release the code upon acceptance.

Guidelines:

- The answer NA means that paper does not include experiments requiring code.
- Please see the NeurIPS code and data submission guidelines (`https://nips.cc/public/guides/CodeSubmissionPolicy`) for more details.
- While we encourage the release of code and data, we understand that this might not be possible, so "No" is an acceptable answer. Papers cannot be rejected simply for not including code, unless this is central to the contribution (e.g., for a new open-source benchmark).
- The instructions should contain the exact command and environment needed to run to reproduce the results. See the NeurIPS code and data submission guidelines (`https://nips.cc/public/guides/CodeSubmissionPolicy`) for more details.
- The authors should provide instructions on data access and preparation, including how to access the raw data, preprocessed data, intermediate data, and generated data, etc.
- The authors should provide scripts to reproduce all experimental results for the new proposed method and baselines. If only a subset of experiments are reproducible, they should state which ones are omitted from the script and why.
- At submission time, to preserve anonymity, the authors should release anonymized versions (if applicable).
- Providing as much information as possible in supplemental material (appended to the paper) is recommended, but including URLs to data and code is permitted.

6. **Experimental setting/details**

Question: Does the paper specify all the training and test details (e.g., data splits, hyperparameters, how they were chosen, type of optimizer, etc.) necessary to understand the results?

Answer: [Yes]

Justification: We have specified all the training and test details in the methodology and experiment section.

Guidelines:

- The answer NA means that the paper does not include experiments.
- The experimental setting should be presented in the core of the paper to a level of detail that is necessary to appreciate the results and make sense of them.
- The full details can be provided either with the code, in appendix, or as supplemental material.

7. **Experiment statistical significance**

Question: Does the paper report error bars suitably and correctly defined or other appropriate information about the statistical significance of the experiments?

Answer: [Yes]

Justification: Our method uses "% Out" in In the experiments section to denote the percentage of pixels with an End-Point Error (EPE) greater than 3 pixels, which effectively reflects the statistical significance of different approaches.

Guidelines:

- The answer NA means that the paper does not include experiments.
- The authors should answer "Yes" if the results are accompanied by error bars, confidence intervals, or statistical significance tests, at least for the experiments that support the main claims of the paper.

- The factors of variability that the error bars are capturing should be clearly stated (for example, train/test split, initialization, random drawing of some parameter, or overall run with given experimental conditions).
- The method for calculating the error bars should be explained (closed form formula, call to a library function, bootstrap, etc.)
- The assumptions made should be given (e.g., Normally distributed errors).
- It should be clear whether the error bar is the standard deviation or the standard error of the mean.
- It is OK to report 1-sigma error bars, but one should state it. The authors should preferably report a 2-sigma error bar than state that they have a 96% CI, if the hypothesis of Normality of errors is not verified.
- For asymmetric distributions, the authors should be careful not to show in tables or figures symmetric error bars that would yield results that are out of range (e.g. negative error rates).
- If error bars are reported in tables or plots, The authors should explain in the text how they were calculated and reference the corresponding figures or tables in the text.

8. **Experiments compute resources**

   Question: For each experiment, does the paper provide sufficient information on the computer resources (type of compute workers, memory, time of execution) needed to reproduce the experiments?

   Answer: [Yes]

   Justification: In the implementation details, we have provided the resource configuration specifications of the computers for each experiment..

   Guidelines:

   - The answer NA means that the paper does not include experiments.
   - The paper should indicate the type of compute workers CPU or GPU, internal cluster, or cloud provider, including relevant memory and storage.
   - The paper should provide the amount of compute required for each of the individual experimental runs as well as estimate the total compute.
   - The paper should disclose whether the full research project required more compute than the experiments reported in the paper (e.g., preliminary or failed experiments that didn't make it into the paper).

9. **Code of ethics**

   Question: Does the research conducted in the paper conform, in every respect, with the NeurIPS Code of Ethics `https://neurips.cc/public/EthicsGuidelines`?

   Answer: [Yes]

   Justification: Our paper is in full compliance with the NeurIPS Code of Ethics.

   Guidelines:

   - The answer NA means that the authors have not reviewed the NeurIPS Code of Ethics.
   - If the authors answer No, they should explain the special circumstances that require a deviation from the Code of Ethics.
   - The authors should make sure to preserve anonymity (e.g., if there is a special consideration due to laws or regulations in their jurisdiction).

10. **Broader impacts**

    Question: Does the paper discuss both potential positive societal impacts and negative societal impacts of the work performed?

    Answer: [NA]

    Justification: There is no societal impact of the work performed.

    Guidelines:

    - The answer NA means that there is no societal impact of the work performed.

- If the authors answer NA or No, they should explain why their work has no societal impact or why the paper does not address societal impact.
- Examples of negative societal impacts include potential malicious or unintended uses (e.g., disinformation, generating fake profiles, surveillance), fairness considerations (e.g., deployment of technologies that could make decisions that unfairly impact specific groups), privacy considerations, and security considerations.
- The conference expects that many papers will be foundational research and not tied to particular applications, let alone deployments. However, if there is a direct path to any negative applications, the authors should point it out. For example, it is legitimate to point out that an improvement in the quality of generative models could be used to generate deepfakes for disinformation. On the other hand, it is not needed to point out that a generic algorithm for optimizing neural networks could enable people to train models that generate Deepfakes faster.
- The authors should consider possible harms that could arise when the technology is being used as intended and functioning correctly, harms that could arise when the technology is being used as intended but gives incorrect results, and harms following from (intentional or unintentional) misuse of the technology.
- If there are negative societal impacts, the authors could also discuss possible mitigation strategies (e.g., gated release of models, providing defenses in addition to attacks, mechanisms for monitoring misuse, mechanisms to monitor how a system learns from feedback over time, improving the efficiency and accessibility of ML).

11. **Safeguards**

    Question: Does the paper describe safeguards that have been put in place for responsible release of data or models that have a high risk for misuse (e.g., pretrained language models, image generators, or scraped datasets)?

    Answer: [NA]

    Justification: The paper poses no such risks

    Guidelines:

    - The answer NA means that the paper poses no such risks.
    - Released models that have a high risk for misuse or dual-use should be released with necessary safeguards to allow for controlled use of the model, for example by requiring that users adhere to usage guidelines or restrictions to access the model or implementing safety filters.
    - Datasets that have been scraped from the Internet could pose safety risks. The authors should describe how they avoided releasing unsafe images.
    - We recognize that providing effective safeguards is challenging, and many papers do not require this, but we encourage authors to take this into account and make a best faith effort.

12. **Licenses for existing assets**

    Question: Are the creators or original owners of assets (e.g., code, data, models), used in the paper, properly credited and are the license and terms of use explicitly mentioned and properly respected?

    Answer: [Yes]

    Justification: The creators or original owners of all assets used in this paper, including code, data, and models, have been properly credited.

    Guidelines:

    - The answer NA means that the paper does not use existing assets.
    - The authors should cite the original paper that produced the code package or dataset.
    - The authors should state which version of the asset is used and, if possible, include a URL.
    - The name of the license (e.g., CC-BY 4.0) should be included for each asset.
    - For scraped data from a particular source (e.g., website), the copyright and terms of service of that source should be provided.

- If assets are released, the license, copyright information, and terms of use in the package should be provided. For popular datasets, `paperswithcode.com/datasets` has curated licenses for some datasets. Their licensing guide can help determine the license of a dataset.
- For existing datasets that are re-packaged, both the original license and the license of the derived asset (if it has changed) should be provided.
- If this information is not available online, the authors are encouraged to reach out to the asset's creators.

13. **New assets**

    Question: Are new assets introduced in the paper well documented and is the documentation provided alongside the assets?

    Answer: [Yes]

    Justification: We have provided enough introduction and documentation.

    Guidelines:

    - The answer NA means that the paper does not release new assets.
    - Researchers should communicate the details of the dataset/code/model as part of their submissions via structured templates. This includes details about training, license, limitations, etc.
    - The paper should discuss whether and how consent was obtained from people whose asset is used.
    - At submission time, remember to anonymize your assets (if applicable). You can either create an anonymized URL or include an anonymized zip file.

14. **Crowdsourcing and research with human subjects**

    Question: For crowdsourcing experiments and research with human subjects, does the paper include the full text of instructions given to participants and screenshots, if applicable, as well as details about compensation (if any)?

    Answer: [NA]

    Justification: The paper does not involve crowdsourcing nor research with human subjects.

    Guidelines:

    - The answer NA means that the paper does not involve crowdsourcing nor research with human subjects.
    - Including this information in the supplemental material is fine, but if the main contribution of the paper involves human subjects, then as much detail as possible should be included in the main paper.
    - According to the NeurIPS Code of Ethics, workers involved in data collection, curation, or other labor should be paid at least the minimum wage in the country of the data collector.

15. **Institutional review board (IRB) approvals or equivalent for research with human subjects**

    Question: Does the paper describe potential risks incurred by study participants, whether such risks were disclosed to the subjects, and whether Institutional Review Board (IRB) approvals (or an equivalent approval/review based on the requirements of your country or institution) were obtained?

    Answer: [NA]

    Justification: The paper does not involve crowdsourcing nor research with human subjects.

    Guidelines:

    - The answer NA means that the paper does not involve crowdsourcing nor research with human subjects.
    - Depending on the country in which research is conducted, IRB approval (or equivalent) may be required for any human subjects research. If you obtained IRB approval, you should clearly state this in the paper.

- We recognize that the procedures for this may vary significantly between institutions and locations, and we expect authors to adhere to the NeurIPS Code of Ethics and the guidelines for their institution.
- For initial submissions, do not include any information that would break anonymity (if applicable), such as the institution conducting the review.

16. **Declaration of LLM usage**

    Question: Does the paper describe the usage of LLMs if it is an important, original, or non-standard component of the core methods in this research? Note that if the LLM is used only for writing, editing, or formatting purposes and does not impact the core methodology, scientific rigorousness, or originality of the research, declaration is not required.

    Answer: [NA]

    Justification: We only use LLM for writing modification.

    Guidelines:

    - The answer NA means that the core method development in this research does not involve LLMs as any important, original, or non-standard components.
    - Please refer to our LLM policy (`https://neurips.cc/Conferences/2025/LLM`) for what should or should not be described.

Appendix

A Network Architecture

Our network adopts a simple MLP architecture that takes spatial-temporal coordinates $(\mathbf{x}, t)$ as input and outputs optical flow signal $\mathbf{u} = (u, v)$. Compared to [19, 27, 32, 36, 37, 63], this coordinate-based MLP implicitly represents optical flow at spatial-temporal coordinates, essentially a velocity field, without relying on explicit discrete structures (e.g., voxel grid, event count image), enabling temporally continuous and dense flow estimation.

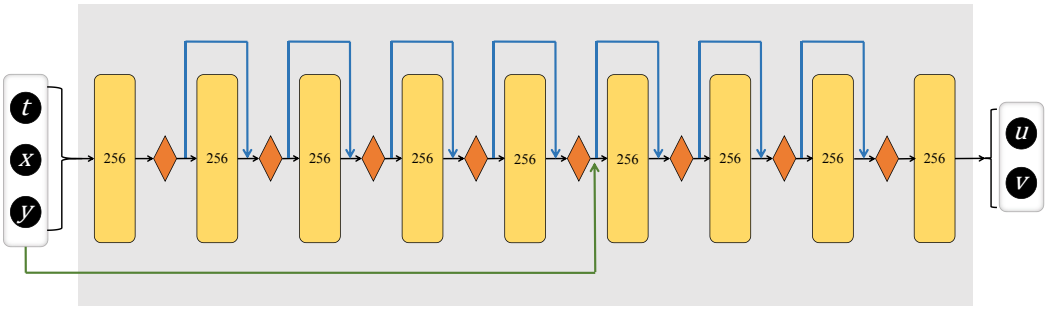

Figure 7: **Schematic Diagram of the Neural Implicit Optical Flow Field Network Architecture.** The input of the network is three-channel spatial-temporal coordinates $(\mathbf{x}, t)$, and the output is optical flow $\mathbf{u} = (u, v)$. The yellow rectangles represent 256-dimensional hidden units. The orange diamonds denote ReLU activation functions. The blue arrows indicate residual connections. The green arrows represent concatenating the original input to the output of the fifth layer.

Specifically, our network architecture, inspired by NeRF [69], employs 9 fully-connected layers with 256 dimensional hidden units. The first eight layers utilize ReLU activations to enforce a low Lipschitz constant, ensuring smoother responses to input variations [70], [71]. This design suppresses high-frequency features while favoring learning of low-frequency features, aligning with the prior that optical flow exhibits spatial-temporal smoothness [17–19]. Notably, no activation function (e.g., ReLU or sigmoid) is applied to the output layer, as optical flow inherently spans both positive and negative values. To further stabilize network training, we introduce residual connections between the second layer to the eighth layer and implement skip connections that concatenate the raw input with the activation outputs of fifth layer. The complete architecture is illustrated in 7.

Although the original NeRF architecture employs positional encoding that enhances high-frequency feature learning [69], our framework deliberately omits such encoding. This design aligns with our goal to model optical flow field which is inherently low-frequency spatial-temporal signals, while avoiding spectral bias toward high-frequency feature [72].

B Continuous Motion Representation

In this section, we discuss how to select an appropriate motion parameterization $\mathcal{F}$ based on the characteristics of camera egomotion. Given a time t, $\mathcal{F}$ maps it to the camera's angular velocity $\boldsymbol{\omega}$ and linear velocity $\boldsymbol{\nu}$ at that moment.

$$\mathcal{F}\colon t \to (\boldsymbol{\omega}, \boldsymbol{\nu}), \quad \mathbb{R} \to \mathbb{R}^3 \times \mathbb{R}^3 \tag{11}$$

In scenarios such as drones, handheld devices, and vehicle-mounted systems, camera ego-motion is constrained by strong prior assumptions. Specifically, camera motion exhibits temporal continuity and smoothness, meaning no abrupt changes occur within infinitesimal time intervals Δt. This prior is formalized as:

$$\frac{d^k \mathcal{F}}{dt^k} \leq O_k, \quad k \in \{0, 1, 2, \ldots, K\} \tag{12}$$

k denotes the order of the derivative and O specifies the upper bounds for their respective derivatives. The equation indicates that the k-th order motion derivatives exist and are continuous. This can be

simplified as:

$$\mathcal{F} \in \mathcal{C}^k \tag{13}$$

$\mathcal{C}^k$ denotes the set of functions that have continuous derivatives up to the k-th order. Additionally, the motion of the camera is low-dimensional [2]. Thus, there is no need to over-parameterize the camera motion (e.g., using neural networks).

In summary, we employ cubic B-spline as $\mathcal{F}$ to parameterize the camera motion, as its basis functions exhibit $\mathcal{C}^2$ continuity and compact representation via sparse control knots [20]. Specifically, we use four control knots $\beta = [\beta_0, \beta_1, \beta_2, \beta_3]^T \in \mathbb{R}^{4\times 6}$ over a time interval $t \in [0, 1]$. Therefore, the motion parameterization $\mathcal{F}$ can be formally defined as:

$$\begin{aligned} \mathcal{F}(t) &= (\boldsymbol{\omega}_\beta(t), \boldsymbol{\nu}_\beta(t)) \in \mathbb{R}^3 \times \mathbb{R}^3 \\ \boldsymbol{\omega}_\beta(t) &= [\,\mathbf{B}(t)\;\beta\,]_{0:2} \\ \boldsymbol{\nu}_\beta(t) &= [\,\mathbf{B}(t)\;\beta\,]_{3:5} \end{aligned} \tag{14}$$

This definition allows us to derive the camera's angular velocity $\boldsymbol{\omega}_\beta(t)$ and linear velocity $\boldsymbol{\nu}_\beta(t)$ at time t, where $\mathbf{B}(t) \in \mathbb{R}^{1\times 4}$ denotes the cubic B-spline basis functions, defined as follows:

$$\mathbf{B}(t) = \frac{1}{6}\begin{bmatrix} t^3 & t^2 & t & 1 \end{bmatrix} \begin{bmatrix} -1 & 3 & -3 & 1 \\ 3 & -6 & 3 & 0 \\ -3 & 0 & 3 & 0 \\ 1 & 4 & 1 & 0 \end{bmatrix} \tag{15}$$

This design choice inherently satisfies the prior assumptions: 1) Cubic B-spline intrinsically enforces $\mathcal{C}^2$ smoothness priors, ensuring natural continuity in velocity, acceleration and jerk without requiring explicit smoothness constraints. 2) By utilizing sparse control knots, this approach model continuous camera motion while maintaining a low-dimensional parameterization of the 6-DoF egomotion.

C Differential Geometric Loss

In 3D vision, the motion of the camera $(\boldsymbol{\omega}, \boldsymbol{\nu})$ induces a motion field $\mathbf{m}$ of projected points on the normalized image plane $\mathbf{x}$. Assuming the camera is a rigid body, the relationship between the motion field and the camera motion can be expressed by the following equation, which we formulate in homogeneous coordinates:

$$\mathbf{m}(\mathbf{x}) = \frac{1}{Z(\mathbf{x})} A(\mathbf{x})\boldsymbol{\nu} + B(\mathbf{x})\boldsymbol{\omega}, \quad \mathbf{x} = [x, y, 1]^T \tag{16}$$

The matrices $A(\mathbf{x})$ and $B(\mathbf{x})$ are functions of homogeneous image coordinates defined as follows:

$$\boldsymbol{A}(\mathbf{x}) = \begin{bmatrix} -1 & 0 & x \\ 0 & -1 & y \\ 0 & 0 & 0 \end{bmatrix}, \quad \boldsymbol{B}(\mathbf{x}) = \begin{bmatrix} xy & -(1+x^2) & y \\ (1+y^2) & -xy & -x \\ 0 & 0 & 0 \end{bmatrix} \tag{17}$$

In practice, $\mathbf{m}(\mathbf{x})$ is approximated by optical flow field $\mathbf{u}(\mathbf{x}) = [u, v, 0]^T$ under brightness constancy assumption.

$$\mathbf{u}(\mathbf{x}) = \frac{1}{Z(\mathbf{x})} A(\mathbf{x})\boldsymbol{\nu} + B(\mathbf{x})\boldsymbol{\omega} \tag{18}$$

Eq.(18) is a critically important motion field equation, which establishes the relationship between optical flow and camera egomotion [22], [73].

However, the presence of $Z(\mathbf{x})$ in this equation implies that recovering camera motion from optical flow or deriving optical flow from camera motion requires knowledge of depth values at each image coordinate. Prior works such as [14, 15, 40–42], rely on depth priors or assume locally shared depth values when performing 6-DOF motion estimation, while methods like [16, 19, 48] jointly estimate depth alongside optical flow and 6-DOF motion. However, this expands the parameterization space of the optimization problem, introducing additional degrees of freedom that may lead to convergence to local minima. Therefore, to enable the formulation of an unsupervised loss function that can simultaneously estimate optical flow and 6-DOF motion with high accuracy, we need to eliminate the dependence on $Z(\mathbf{x})$.

Table 5: **Ablation studies on early stopping strategy.**

		indoor_flying1	indoor_flying2	indoor_flying3	outdoor_day1
Time	w/o early stopping	9.30s	9.41s	9.50s	10.77s
	w/ early stopping	4.21s	4.30s	4.87s	4.56s
	efficiency improvement	2.21× ↑	2.19× ↑	1.99× ↑	2.36× ↑
EPE	w/o early stopping	1.58	2.04	1.84	1.63
	w/ early stopping	1.61	2.09	1.90	1.68
	performance drop	1.90% ↓	2.45% ↓	3.26% ↓	3.07% ↓

We transpose Eq.(18) and then left-multiply by $\boldsymbol{\nu} \times \mathbf{x}$, form the inner product of $\mathbf{u}(\mathbf{x})$ and $\boldsymbol{\nu} \times \mathbf{x}$, yieding a scalar equation to isolate $Z(\mathbf{x})$ as follows. $\times$ denotes the cross product operation.

$$\mathbf{u}(\mathbf{x})^T (\boldsymbol{\nu} \times \mathbf{x}) = \left(\frac{1}{Z(\mathbf{x})} A(\mathbf{x}) \boldsymbol{\nu} + B(\mathbf{x}) \boldsymbol{\omega} \right) (\boldsymbol{\nu} \times \mathbf{x}) \tag{19}$$

Simplify the above equation to obtain:

$$\mathbf{u}(\mathbf{x})^T [\boldsymbol{\nu}]_\times \mathbf{x} = \frac{1}{Z(\mathbf{x})} \boldsymbol{\nu}^T A(\mathbf{x})^T [\boldsymbol{\nu}]_\times \mathbf{x} + \boldsymbol{\omega}^T B(\mathbf{x})^T [\boldsymbol{\nu}]_\times \mathbf{x} \tag{20}$$

where $[\cdot]_\times$ denotes the skew-symmetric operation. Interestingly, it can be proven that the coefficient of the term that involves $Z(\mathbf{x})$ in Eq.(20) is identically zero.

$$\boldsymbol{\nu}^T A(\mathbf{x})^T [\boldsymbol{\nu}]_\times \mathbf{x} \equiv 0 \tag{21}$$

Therefore, Eq.(20) can be further simplified as follows:

$$\mathbf{u}(\mathbf{x})^T [\boldsymbol{\nu}]_\times \mathbf{x} - \boldsymbol{\omega}^T B(\mathbf{x})^T [\boldsymbol{\nu}]_\times \mathbf{x} = 0 \tag{22}$$

By expanding $\boldsymbol{\omega}^T B(\mathbf{x})^T [\boldsymbol{\nu}]_\times \mathbf{x}$, Eq.(22) can be rewritten in the following form:

$$\mathbf{u}(\mathbf{x})^T [\boldsymbol{\nu}]_\times \mathbf{x} - \mathbf{x}^T \mathbf{s} \mathbf{x} = 0, \quad \mathbf{s} = \frac{1}{2} \left([\boldsymbol{\omega}]_\times [\boldsymbol{\nu}]_\times + [\boldsymbol{\nu}]_\times [\boldsymbol{\omega}]_\times \right) \tag{23}$$

Finally, we obtained an equation that connects the optical flow field and camera motion without relying on depth values.Eq.(23) can theoretically be regarded as a differential form of the epipolar constraint. We use this as our differential geometric loss to jointly learn optical flow and 6-DoF motion, as shown in the following equation.

$$\begin{aligned} L_{\text{geometry}}(t, \mathbf{x}, \theta, \beta) &= \left\| \mathbf{u}_\theta(t, \mathbf{x})^T [\boldsymbol{\nu}_\beta(t)]_\times \mathbf{x} - \mathbf{x}^T \mathbf{s}_\beta(t) \mathbf{x} \right\|_2^2, \\ \mathbf{s}_\beta(t) &= \frac{1}{2} \left([\boldsymbol{\omega}_\beta(t)]_\times [\boldsymbol{\nu}_\beta(t)]_\times + [\boldsymbol{\nu}_\beta(t)]_\times [\boldsymbol{\omega}_\beta(t)]_\times \right) \end{aligned} \tag{24}$$

Here, $\mathbf{u}_\theta(t, \mathbf{x})$ represents the optical flow obtained from our neural implicit representation, while $\boldsymbol{\omega}_\beta(t)$ and $\boldsymbol{\nu}_\beta(t)$ denote the angular velocity and linear velocity of the camera, derived from the cubic B-spline continuous motion representation.

D More Ablation Studies

Early Stopping Strategy. To enhance computational efficiency, we employed the early-stopping strategy from [52–54] on the MVSEC dataset [64] under $dt = 4$. Specifically, we set the patience to 45 and the minimum improvement threshold to 1×10^{-3}, applying the early stopping strategy after 300 iterations. The results in Tab. 5 indicate that the training speed was boosted by 2.2x, while the optical flow estimation accuracy showed only a slight 2.67% drop in the EPE. This demonstrates that the strategy significantly reduces training time at the cost of only a minor loss in accuracy, achieving an excellent trade-off.

E More Qualitative Results

We further provide additional qualitative results. As shown in 8, our method achieves comprehensive 6-DoF motion estimation on the MVSEC dataset [64]. The angular velocity and linear velocity estimated by our approach closely match the ground-truth motion.

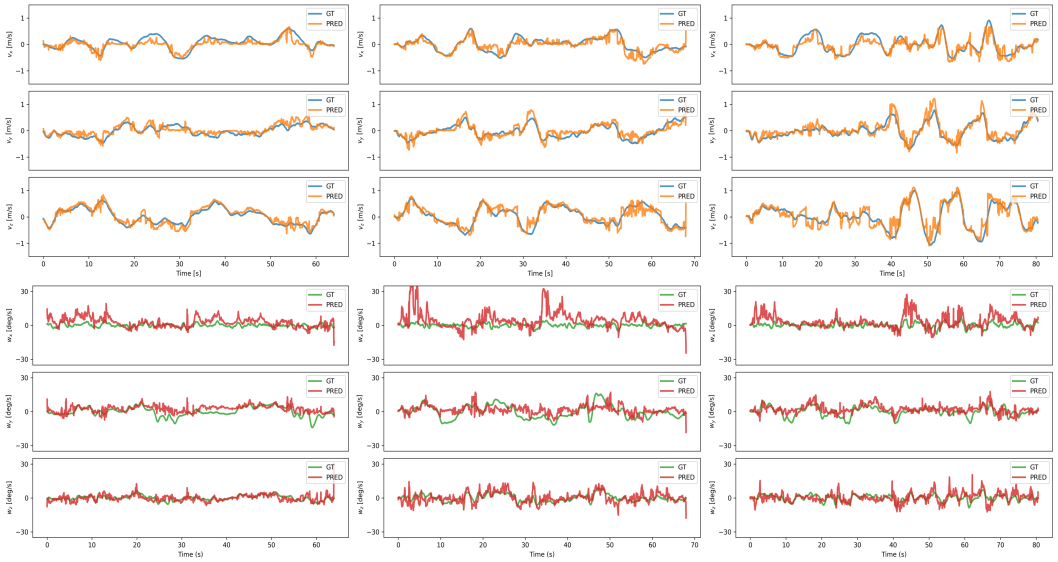

indoor flying1 indoor flying2 indoor flying3

Figure 8: **Complete qualitative results of 6-DoF motion estimation on the MVSEC dataset.** The top section displays the linear velocity estimation results (in m/s), while the bottom section shows the angular velocity estimation results (in deg$/s$). The top, middle, and bottom rows in each subfigure correspond to the x-axis, y-axis, and z-axis results, respectively.

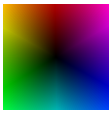

Figure 9: **Color wheel for visualizing optical flow.** A green color in the optical flow visualization corresponds to motion directed toward the lower-left corner of the image, while the saturation of the color encodes the flow magnitude — more vivid hues indicate larger displacement values.

For MVSEC datasets [64], We provide additional qualitative comparisons of optical flow estimation between our method and MultiCM [17], the second-best performing baseline. As shown in 10, our approach predicts optical flow with superior continuity and smoothness, validating the effectiveness of our neural implicit optical flow field representation. The color wheel used to visualize optical flow is shown in 9, where different colors encode the magnitude and direction of the optical flow.

For DSEC datasets [68], We provide additional visualization comparisons of optical flow estimation between our method, state-of-the-art unsupervised learning methods, and supervised learning methods on more sequences. The results in Fig. 11 demonstrate that in some scenarios, our method yields visually superior results with smoother optical flow, while in scenes with complex textures and drastic depth changes, it may produce errors at the edges.

Furthermore, we also provide visualization results of the flow field in $X - Y - T$ 3D space on the MVSEC dataset [64]. The results in Fig. 12 indicate that our method exhibits an emergent capability for point tracking, which is the ability to track the movement of points in pixel space.

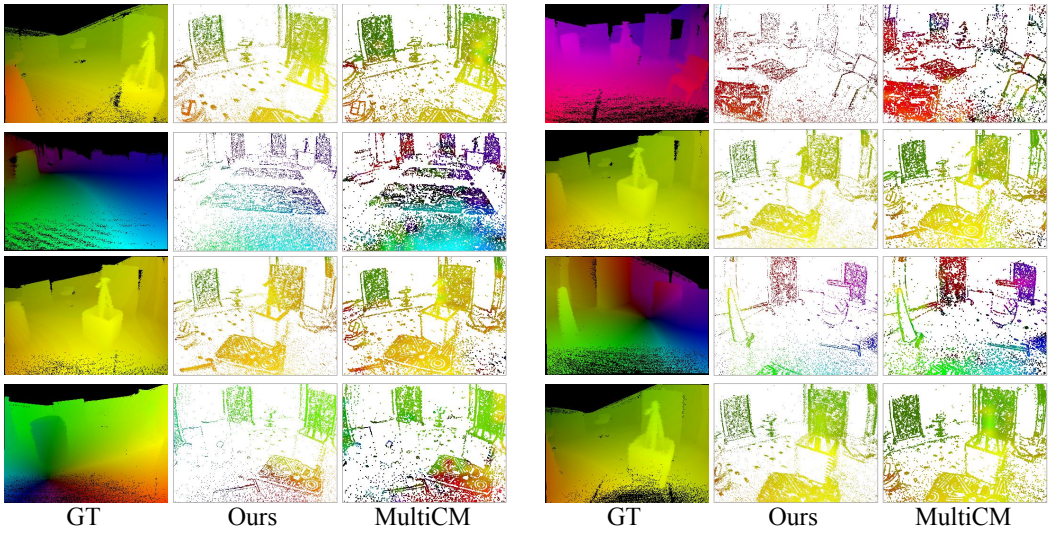

Figure 10: **More qualitative results of optical flow estimation on the MVSEC dataset.** It can be clearly observed that our method estimates smoother optical flow, free from abrupt variations, and demonstrates closer alignment with the ground truth optical flow. This indicates that our approach more effectively models the intrinsically spatial-temporally continuous optical flow field.

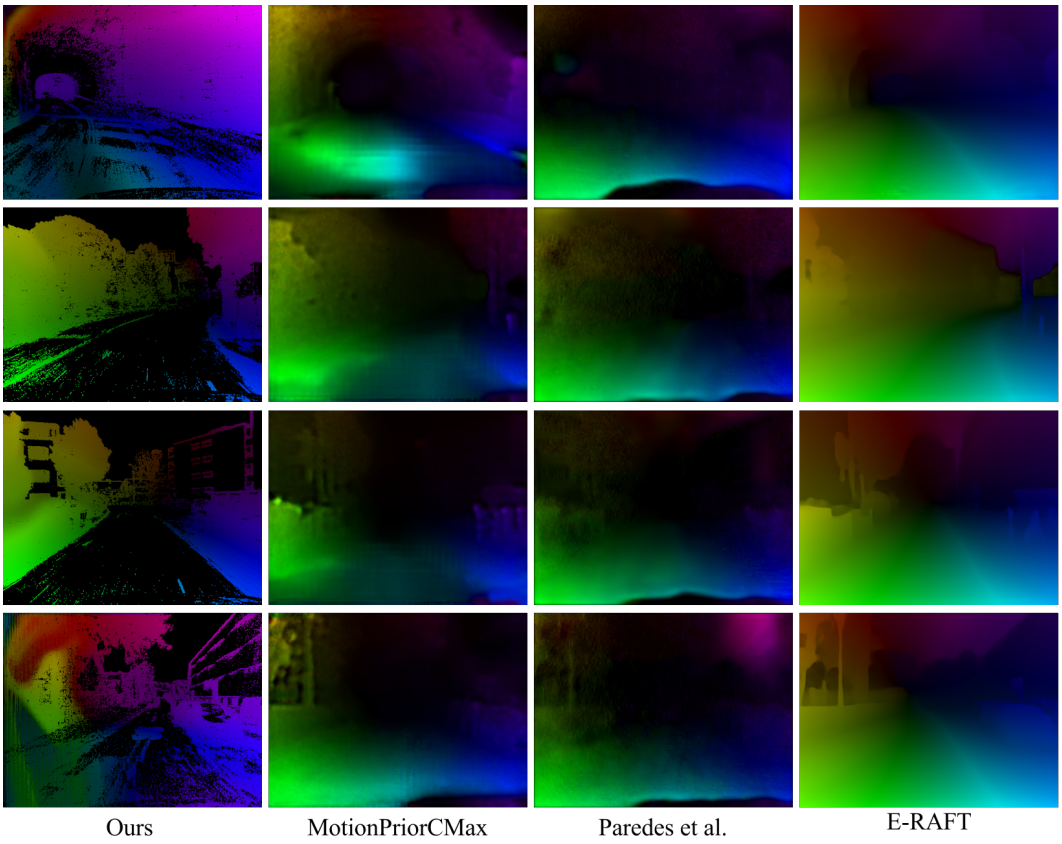

Figure 11: **More qualitative results of optical flow estimation on the DSEC dataset.** Qualitative results of optical flow estimation on the DSEC dataset. The results in the first, second, third, and fourth rows correspond to sequences *interlaken_00b*, *thun_01a*, *thun_01a*, and *zurich_city_14a* respectively.

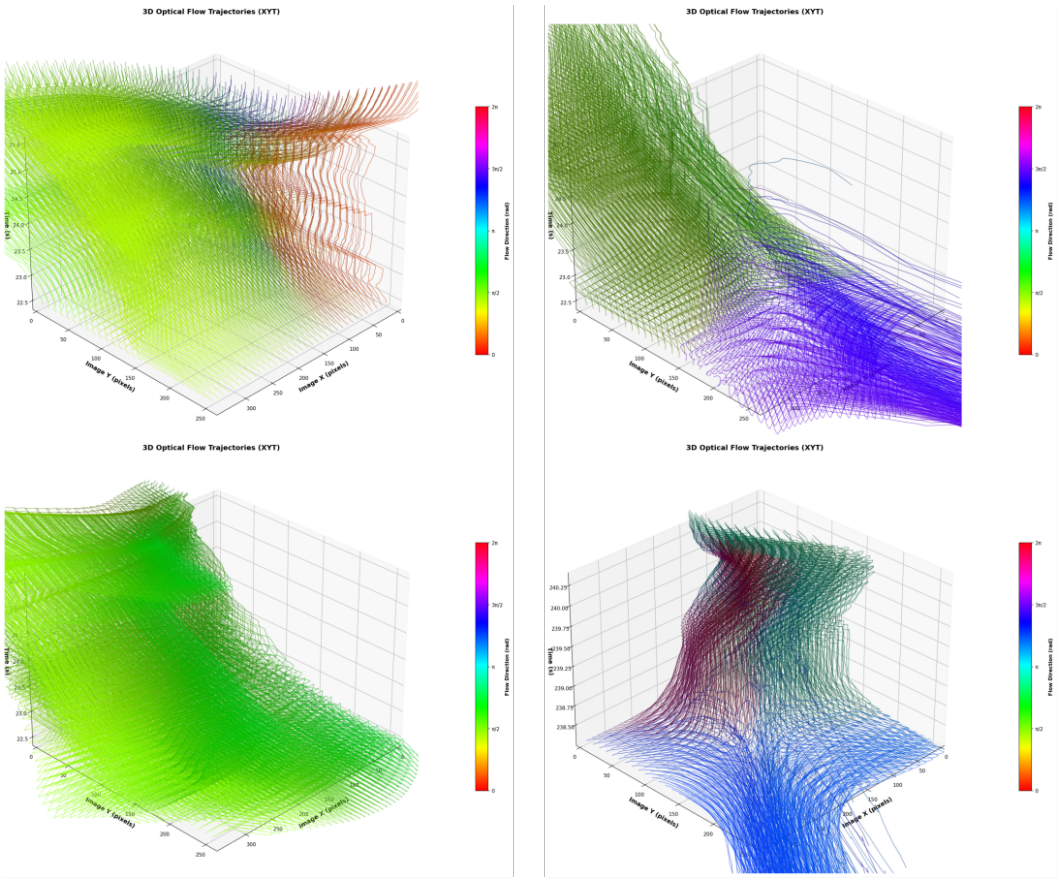

Figure 12: **Point tracking results of flow field on the MVSEC dataset.**